Localized Time-Resolved Electron-Temperature Measurements Indicate Nonuniformly Driven Two-Plasmon–Decay Instability in Direct-Drive Implosions

The two-plasmon–decay (TPD) instability is the decay of an incident laser photon into two plasmons[1,2] that can generate energetic electrons, thereby preheating direct-drive inertial confinement fusion (ICF)[3,4] implosions and degrading their performance. The phase-matching conditions for this instability restrict it to electron densities of $n_e \le n_c/4$, where n_c is the critical density at which the plasma frequency equals the laser frequency. This instability is generally accompanied by optical emission near $\omega_0/2$ and $3\omega_0/2$, where ω_0 is the laser frequency. Above the TPD threshold, energetic electron production is frequently observed as evidenced by hard x-ray emission.

Various aspects of the half-harmonic emission from laser-produced plasmas were analyzed in 1985 (Ref. 5). In particular, a sharp red-shifted spectral feature was identified as a result of the absolute TPD instability[6] in inhomogeneous plasmas[6–9] that occurs very close to the $n_c/4$ density. This feature is most likely caused by inverse resonance absorption that can efficiently convert the low-frequency TPD plasmons to photons. Since the frequencies of these plasmons depend only on the local electron temperature, this spectral feature also provides a powerful electron-temperature diagnostic[5] in close proximity of the $n_c/4$ surface. Absorption of this feature on the way out of the plasma is significant (80% to 90%), but its intensity is generally sufficient to make it readily observable.

The TPD instability was originally thought to involve only a single laser beam. In 2003, planar-interaction experiments and spherical implosion experiments[10] at LLE demonstrated that the TPD instability was a multibeam instability.[11] At that time there was no theory to explain the multibeam interaction, energetic electron generation, or different onsets for the half-integer harmonics and hard x-ray emission. The spectral extent of the $\omega/2$ and $3\omega/2$ emission indicated that this instability extended well into the convective TPD regime[12–14] to densities limited by Landau damping near $n_e \le n_c/5$ (Ref. 11), where $k_p\lambda_{De} \sim 0.25$ (k_p and λ_{De} are the longer of the two TPD plasmon $\underline{k}$-vectors and the Debye length). Over the past decade, significant progress has been made on multibeam TPD theories and simulations using kinetic particle-in-cell (PIC),[14–16] reduced PIC (RPIC),[17–20] and fluid-type Zakharov simulations.[20–23] These simulations have shown that both absolute and convective TPD instabilities can be driven by multiple beams and that beam configurations (number of beams, angles of incidence, and polarization) determine the outcome. They also showed that within ~10 ps or less, the TPD instability is dominated by nonlinear effects and saturation. This implies that the linear regime of this instability is not observable experimentally.

Recent work at LLE showed the effect of beam configurations, polarization, threshold, and intensity scaling of hot-electron production resulting from TPD[24,25] based on experiments and linear gain calculations.

In this article we present the first precision (~5%), time-resolved electron-temperature measurements in different areas of an imploding target and located in density space between $0.24 < n_e/n_c < 0.25$. These measurements indicate that close to the TPD threshold, the measured temperatures agree well with those predicted by hydrodynamic simulations, while above the threshold, they typically exceed the simulations by up to 20%. The exact amount of the excess temperature depends on the number of overlapping beams that drive the instability in any particular area.

Experiments were carried out on LLE's 60-beam OMEGA Laser System[26] using spherical targets. Each beam illuminates the entire hemisphere of the target using distributed phase plates (DPP's)[27] and smoothing by spectral dispersion (SSD).[28] Time-resolved $\omega/2$ spectra were recorded in three locations: one through one of the beam ports (backscattering) and two centered within a hex or pent port (see Fig. 135.18). The signals from beam and hex ports were collected near the target chamber and fiber optically relayed to a time-multiplexed, 1/3-m spectrometer. The signal from the pent port was optically relayed to a similar spectrometer. Both spectrometers were proximity coupled to ROSS streak cameras.[29] Typical spectral and temporal resolutions were ~1 nm and ~100 ps, respectively. All streak records were routinely corrected for geometric and sweep-speed nonlinearities to near 1% residual

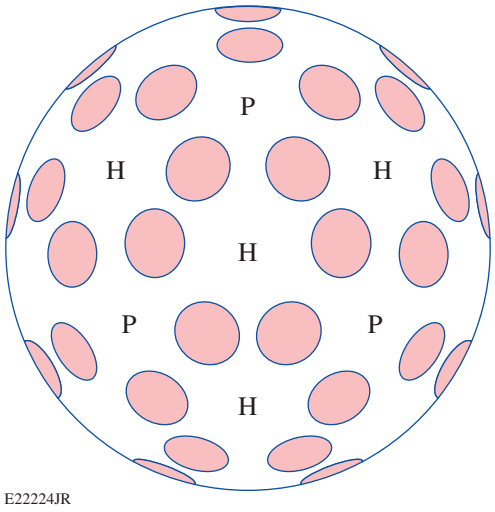

Figure 135.18
Schematic of the OMEGA target chamber with beam ports (shaded) and the locations of hex (H) and pent (P) ports. $\omega/2$ spectra were recorded through one of the beam ports and centered on one of the H and P ports.

nonlinearity. The two multiplexed spectra viewed the entire target sphere, while the spectra recorded in the pent location viewed an ~50-μm × 50-μm area on the target sphere.

Half-harmonic images were recorded on a charge-coupled–device (CCD) camera at the center of another hex port. Colored glass and an interference filter at the camera input integrated over either the entire $\omega/2$ spectrum (680 nm and 720 nm) or only the blue part of the spectrum (680 nm to 700 nm). (The central $\omega_0/2$ wavelength lies at 702 nm.)

Representative $\omega/2$ spectra recorded at the center of the pent port are shown in Fig. 135.19 for two viewing directions: one viewing an imploding target along the target normal [Fig. 135.19(a)]; the other one displaced by ~100 μm and inclined by ~10° relative to the target normal [Fig. 135.19(d)]. The sharp red-shifted spectral feature [Fig. 135.19(a)] is the same as that previously identified with the absolute TPD instability.[5,6] This spectral feature results from plasmon-to-photon conversion[30] via inverse resonance absorption of the lower-frequency TPD plasmons whose k-vectors nearly vanish. The multibeam nature of the instability is inferred from threshold calculations. The absolute TPD threshold[6,23] can be defined as $\eta = 1$, where $\eta = I_{14} L_{n,\mu m} / \left(233\, T_{e,keV}\right)$ and I_{14}, L_n, and T_e are the intensity, density scale length, and electron temperature at $n_c/4$ in units of 10^{14} W/cm^2, μm, and keV, respectively. For the multibeam geometries prevalent on OMEGA, I_{14} represents the sum of all the beam intensities that can contribute to the absolute TPD instability at the point of interest.[23] For the shots shown in Fig. 135.19, the single-beam peak intensity toward the end of the laser pulse was $I_{14} \sim 2.35$, $L_n \sim 100$ μm, and $T_e \sim 1.8$ keV, resulting in $\eta \sim 0.2$, i.e., far below the absolute TPD threshold. Using hydrodynamic predictions for these quantities where I_{14} is the total intensity at quarter critical summed over all angles of incidence, we note that η shown in Fig. 135.19(c) is close to 1, i.e., the threshold. In fact, this average intensity

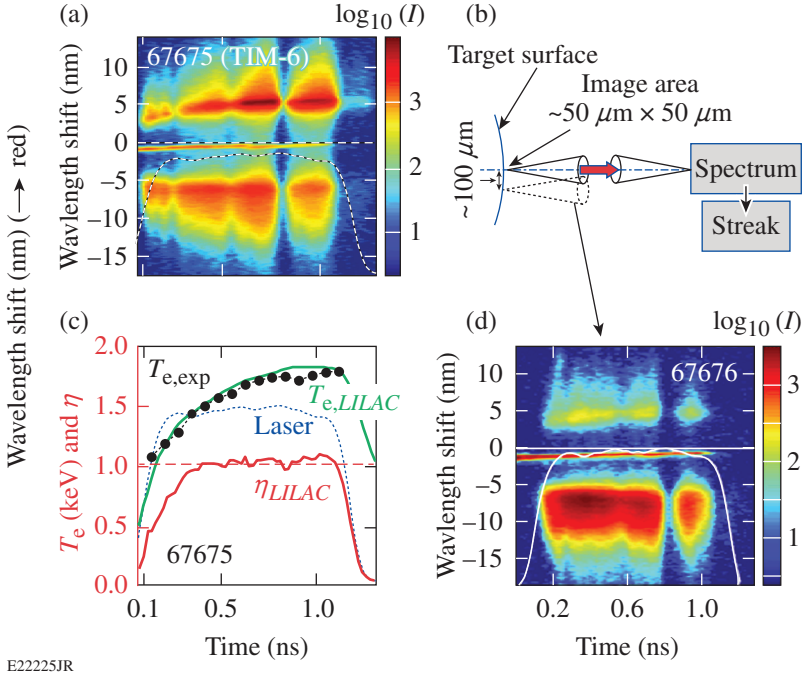

Figure 135.19
Time-resolved $\omega/2$ spectra viewing a small area on the target surface. (a) Spectrum taken along the target normal; (b) schematic setup for time-resolved $\omega/2$ spectroscopy; (c) measured electron temperatures (black dots), *LILAC* predictions (green line), laser power (blue dashed line), and threshold parameter η obtained from *LILAC* (red line); (d) equivalent $\omega/2$ spectrum taken ~10° off the target normal.

is an overestimate of the relevant overlapped intensity that can drive the TPD instability, particularly if polarization smoothing is included, which presumably halves the TPD drive intensity. The discrepancy may be related to the speckle nature of the focal spot for which peak intensities can easily be 3× to 5× larger. The influence of speckles on driving the TPD instability is presently being investigated using the Zakharov simulations.

Figure 135.19(d) shows the off-axis $\omega/2$ spectrum, which is dominated by the broad blue-shifted spectral feature corresponding to TPD decays well below $n_c/4$. These features cannot be generated by mode conversion but require Thomson scattering using one of the irradiation beams as the Thomson probe. For the OMEGA geometry, the phase-matching conditions for generating $\omega/2$ radiation via Thomson scattering are not satisfied for Thomson scattering off primary TPD plasmons using any of the OMEGA beams as the Thomson probe. These conditions can be satisfied, however, if the TPD plasma waves roughly fill k space up to the Landau cutoff density as predicted in the nonlinear evolution of the instability by PIC,[16] RPIC,[18,31] and Zakharov[20,32,33] simulations. In principle, inverse parametric decay could generate some of these spectral features. This process is not very likely since it is a higher-order process involving TPD plasmons and ion waves with appropriate k-vectors.

The broad $\omega/2$ spectral features do not reveal the generation processes but indicate the range of densities involved in the TPD instability. The two TPD plasmons have frequencies $\omega_{1,2} = \omega_0/2 \pm \Delta\omega$. Along the maximum TPD growth-rate curve[5,6,11] $\Delta\omega/\omega_0 = 4.4 \times 10^{-3}\ \kappa T_{e,keV}$, where $\kappa = \mathbf{k}_1 \cdot \mathbf{k}_0/k_0^2 - 1/2$ (Ref. 5), and k_0 and k_1 are the k-vectors of the incident photons and the larger-k plasmon of the two TPD waves. The absolute TPD instability near $n_c/4$ has the lowest single and multibeam thresholds,[6,23,33] corresponding to $\kappa \approx 0.5$ and $T_{e,keV} \approx \Delta\lambda_{nm}/3.1$ for $\lambda_L = 351$ nm. The wavelength shift $\Delta\lambda_{nm}$ of the sharp red-shifted spectra in Fig. 135.19, therefore, indicates an electron temperature at $n_c/4$ of $T_e \approx 1.66$ keV, in good agreement with 1-D hydrodynamic *LILAC*[34] predictions [green line in Fig. 135.19(c)]. Near the Landau cutoff, the frequency shifts are 2× to 3× larger but are of limited diagnostic value since they depend sensitively on the wave vectors probed.

Images of the $\omega/2$ emission provide significant information regarding localization of the TPD instability (Fig. 135.20). Figure 135.20(a) was filtered for the entire $\omega/2$ spectrum (680 nm to 740 nm) for an imploding target at $I_{max} \sim 10^{15}$ W/cm^2, while in Fig. 135.20(b) only the blue $\omega/2$ component was recorded.

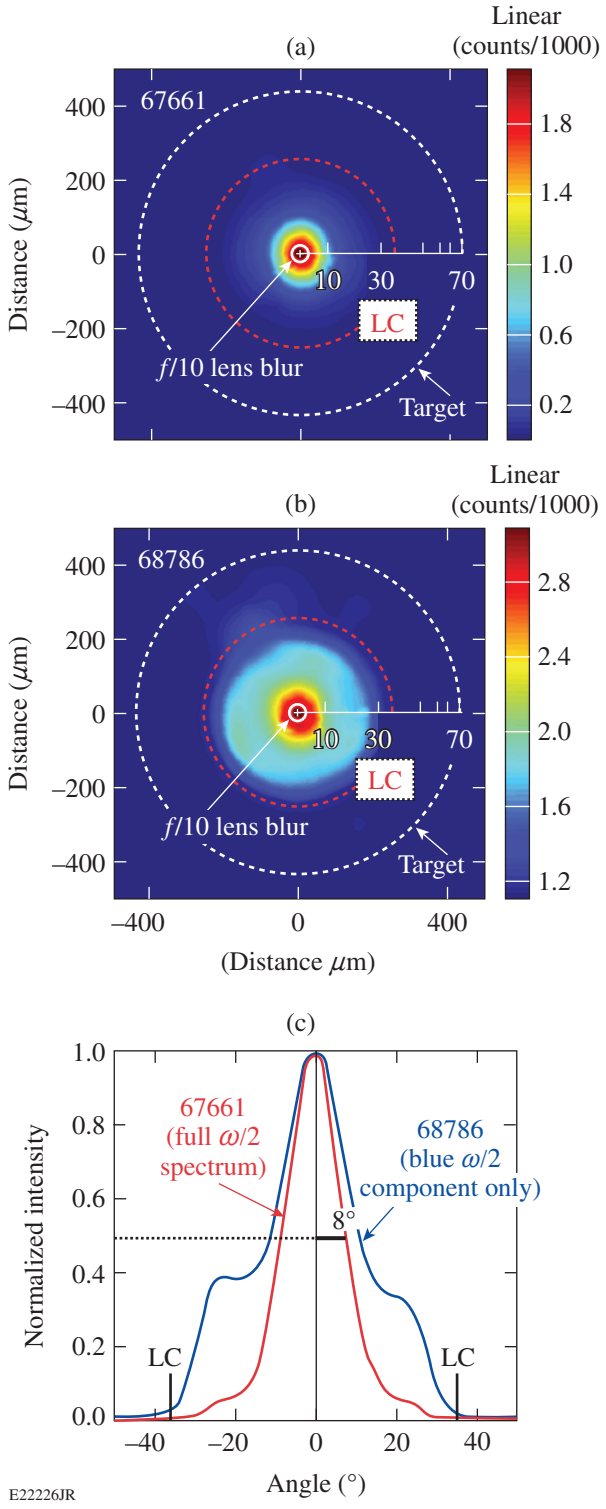

Figure 135.20
The $\omega/2$ images taken through a hex port (surrounded by six beams). (a) Image of an imploding target for 680 nm < λ < 740 nm; (b) same as in (a) but 680 nm < λ < 700 nm; (c) cross-sectional lineouts through the center of the target for (a) and (b). LC: Landau cutoff.

A scale is superposed in Figs. 135.20(a) and 135.20(b) translating the spatial information in the images into emission angles in degrees. Figure 135.20(c) shows two lineouts through the centers of Figs. 135.20(a) and 135.20(b). Figure 135.20(a) is dominated by the sharp red feature that originates very near its critical density. This emission is guided along the density gradient because of the conservation of the wave vector perpendicular to the density gradient in the near-planar density profile. This also explains the narrow emission cone angle in Fig. 135.20(c), which is ~6° after correction for the *f*/10 imaging optics. Assuming planar geometry (valid considering the dimensions and angles involved relative to the curvature of the $n_c/4$ surface), this narrow cone angle can be used to estimate the maximum density from which the sharp red feature may be emitted. This maximum density is $n_e/n_c \approx 0.247$ and includes the density region for the absolute instability,[6] $0.247 < n_e/n_c \leq 0.25$, depending on T_e.

The $\omega/2$ image in Fig. 135.20(b) is consistent with the spectra shown in Fig. 135.19. Since the sharp red feature is not recorded, this image sees only emission from lower densities (larger $\Delta\lambda$) corresponding to larger emission angles. If this source were isotropic over the entire quarter-critical surface, this image intensity would drop off at the polar angle $\theta_{LC} \sim 37°$, determined by refraction of $\omega/2$ light generated at the Landau cutoff. The location of the Landau cutoff is indicated in Fig. 135.20 by LC and the red dashed circles. There is only scant emission at or beyond the Landau cutoff consistent with past Thomson-scattering results.[11] A halo of blue $\omega/2$ emission extends to the Landau cutoff with three areas of increased emission near the 12, 5, and 7 o'clock positions. The former is likely caused by the six beams surrounding the hex port, while the latter correspond to the positions of the three neighboring pent ports (Fig. 135.18) located at $\theta \sim 37.5°$ or right at the Landau cutoff. (The three neighboring hex ports are located 4° farther out and emission from these port locations is not identifiable in these images.) The angular resolution of these images is severely limited by refraction and the large angle emission of the broad $\omega/2$ features. It is therefore impossible to resolve individual beams separated by ~23°.

The relatively narrow central spike in Fig. 135.20(b) (~11° half-cone angle) is consistent with a small TPD interaction area centered on the hex ports. Analogous arguments hold for the pent ports where the thresholds are ~20% higher than in the hex ports (five versus six beams as primary contributors to the instability). In the 60 beam-port locations, four beams can effectively drive the absolute TPD instability, albeit at another 20% increased threshold intensity. The interaction area estimates are very rough since they depend on the nonlinear TPD plasma wave spectrum and the possible experimental Thomson-scattering scenarios on OMEGA.

The onset of $\omega/2$ emission in Fig. 135.21 is consistent with the TPD thresholds[6] if the intensity includes the total number of overlapping beams that can drive the absolute instability at a particular location. At the center of a hex port, six beams overlap but their intensities are reduced by absorption (~10%) on the way to $n_c/4$ and the intensity profile (~10%) for a total intensity of ~4.8× the single-beam peak intensity. Near the center of each beam, four beams can drive the TPD instability (Fig. 135.18). After accounting for absorption and beam profile, the total intensity is ~3.4× the single-beam intensity at this location. (Higher-angle beams contribute insignificantly

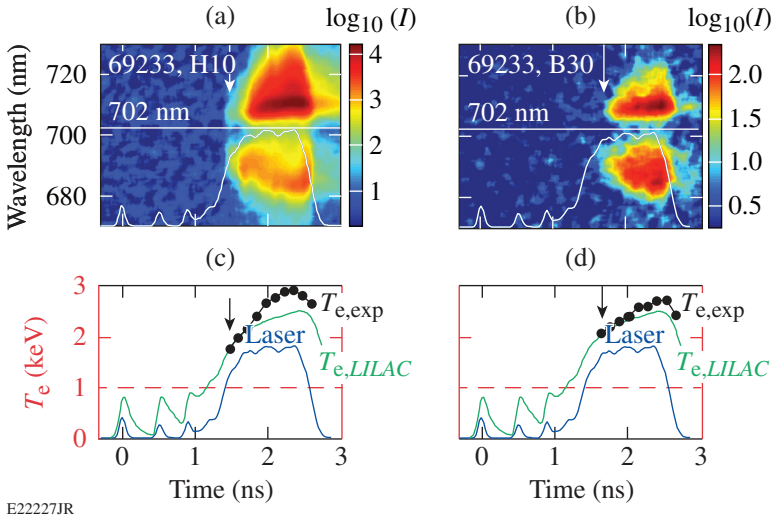

Figure 135.21
The $\omega/2$ spectra taken for an imploding room-temperature target at 9.3×10^{14} W/cm^2 through (a) a beam port and (b) a hex port. The laser pulse shape is shown in each panel. The sharp red-shifted features in (a) and (b) were used to measure T_e in (c) and (d). Random error bars are equal to the symbol sizes. Hydrodynamic predictions for T_e are shown in green. Arrows indicate the onset of $\omega/2$ emission and estimated TPD thresholds.

because of the intensity profiles.) Different onset times for the TPD instability (white and black arrows in Fig. 135.21) are evident in the spectra taken at the beam port and hex port locations. The onsets the T_e increase and corresponding maximum electron temperatures [Fig. 135.21(c)] in the two locations reflect the different absolute TPD thresholds $I_{th} \sim IL_n / T_e$, where I is the overlapped intensity and L_n is density gradient length. Both I and L_n increase with time past $t = 1.5$ ns in Fig. 135.21. The maximum temperatures vary over the quarter-critical surface and locally exceed the average temperatures predicted by hydrodynamic simulations by 10% to 20%. (At the onset of the spectra, the measured temperatures agree well with the hydrodynamic simulations.) The measured temperature excursions beyond the hydrodynamic predictions entail $n_c/4$ surface perturbations caused by pressure uniformity in the corona. Such perturbations have been reproduced in two-dimensional (2-D) hydrodynamic simulations.

In conclusion, spatially and temporally resolved half-harmonic spectra and images of laser-driven implosions show clear evidence for the multibeam nature of the TPD instability, its rapid nonlinear evolution, and its spatially limited extent. The thresholds correspond to the multibeam-driven absolute instability and are identified via a sharp red-shifted spectral feature. These thresholds agree with published absolute thresholds after adjusting the intensity for multibeam effects. The broad $\omega/2$ spectral features that develop essentially simultaneously with the sharp red-shifted feature are identified as the nonlinear phase of the TPD instability that extends rapidly all the way to the Landau cutoff covering the conventionally called convective regime. There is no experimental evidence for a linear convective regime. These results are in good agreement with recent fluid and kinetic TPD simulations. Localized T_e measurements and $\omega/2$ images point toward localized temperature islands near $n_c/4$, where temperatures exceed the average by 10% to 20% and entail localized surface perturbations.

ACKNOWLEDGMENT

This work was supported by the U.S. Department of Energy Office of Inertial Confinement Fusion under Cooperative Agreement No. DE-FC52-08NA28302, the University of Rochester, and the New York State Energy Research and Development Authority. The support of DOE does not constitute an endorsement by DOE of the views expressed in this article.

REFERENCES

1. M. V. Goldman, Ann. Phys. **38**, 95 (1966).
2. M. V. Goldman, Ann. Phys. **38**, 117 (1966).
3. J. D. Lindl, *Inertial Confinement Fusion: The Quest for Ignition and Energy Gain Using Indirect Drive* (Springer-Verlag, New York, 1998).
4. D. W. Phillion *et al.*, Phys. Rev. Lett. **49**, 1405 (1982).
5. W. Seka, B. B. Afeyan, R. Boni, L. M. Goldman, R. W. Short, K. Tanaka, and T. W. Johnston, Phys. Fluids **28**, 2570 (1985).
6. A. Simon, R. W. Short, E. A. Williams, and T. Dewandre, Phys. Fluids **26**, 3107 (1983).
7. C. S. Liu, M. N. Rosenbluth, and R. B. White, Phys. Rev. Lett. **31**, 697 (1973).
8. M. N. Rosenbluth, R. B. White, and C. S. Liu, Phys. Rev. Lett. **31**, 1190 (1973).
9. B. B. Afeyan and E. A. Williams, Phys. Rev. Lett. **75**, 4218 (1995).
10. C. Stoeckl, R. E. Bahr, B. Yaakobi, W. Seka, S. P. Regan, R. S. Craxton, J. A. Delettrez, R. W. Short, J. Myatt, A. V. Maximov, and H. Baldis, Phys. Rev. Lett. **90**, 235002 (2003).
11. W. Seka, D. H. Edgell, J. F. Myatt, A. V. Maximov, R. W. Short, V. N. Goncharov, and H. A. Baldis, Phys. Plasmas **16**, 052701 (2009).
12. M. N. Rosenbluth, Phys. Rev. Lett. **29**, 565 (1972).
13. L. V. Powers and R. L. Berger, Phys. Fluids **28**, 2419 (1985).
14. R. Yan, A. V. Maximov, and C. Ren, Phys. Plasmas **17**, 052701 (2010).
15. R. Yan, A. V. Maximov, C. Ren, and F. S. Tsung, Phys. Rev. Lett. **103**, 175002 (2009).
16. R. Yan, C. Ren, J. Li, A. V. Maximov, W. B. Mori, Z. M. Sheng, and F. S. Tsung, Phys. Rev. Lett. **108**, 175002 (2012).
17. H. X. Vu, D. F. DuBois, D. A. Russell, and J. F. Myatt, Phys. Plasmas **17**, 072701 (2010).
18. H. X. Vu, D. F. DuBois, J. F. Myatt, and D. A. Russell, Phys. Plasmas **19**, 102703 (2012).
19. H. X. Vu, D. F. DuBois, D. A. Russell, and J. F. Myatt, Phys. Plasmas **19**, 102708 (2012).
20. J. F. Myatt, J. Zhang, J. A. Delettrez, A. V. Maximov, R. W. Short, W. Seka, D. H. Edgell, D. F. DuBois, D. A. Russell, and H. X. Vu, Phys. Plasmas **19**, 022707 (2012).
21. D. A. Russell and D. F. DuBois, Phys. Rev. Lett. **86**, 428 (2001).
22. J. F. Myatt, H. X. Vu, D. F. DuBois, D. A. Russell, J. Zhang, R. W. Short, and A. V. Maximov, Phys. Plasmas **20**, 052705 (2013).
23. J. Zhang, J. F. Myatt, R. W. Short, A. V. Maximov, H. X. Vu, D. F. DuBois, and D. A. Russell, "Multibeam Two-Plasmon Decay from Linear Threshold to Nonlinear Saturations," to be submitted to Physical Review Letters.
24. D. T. Michel, A. V. Maximov, R. W. Short, J. A. Delettrez, D. Edgell, S. X. Hu, I. V. Igumenshchev, J. F. Myatt, A. A. Solodov, C. Stoeckl, B. Yaakobi, and D. H. Froula, Phys. Plasmas **20**, 055703 (2013).

25. D. T. Michel, A. V. Maximov, R. W. Short, S. X. Hu, J. F. Myatt, W. Seka, A. A. Solodov, B. Yaakobi, and D. H. Froula, Phys. Rev. Lett. **109**, 155007 (2012).

26. T. R. Boehly, D. L. Brown, R. S. Craxton, R. L. Keck, J. P. Knauer, J. H. Kelly, T. J. Kessler, S. A. Kumpan, S. J. Loucks, S. A. Letzring, F. J. Marshall, R. L. McCrory, S. F. B. Morse, W. Seka, J. M. Soures, and C. P. Verdon, Opt. Commun. **133**, 495 (1997).

27. Y. Lin, T. J. Kessler, and G. N. Lawrence, Opt. Lett. **20**, 764 (1995).

28. S. Skupsky, R. W. Short, T. Kessler, R. S. Craxton, S. Letzring, and J. M. Soures, J. Appl. Phys. **66**, 3456 (1989).

29. W. R. Donaldson, R. Boni, R. L. Keck, and P. A. Jaanimagi, Rev. Sci. Instrum. **73**, 2606 (2002).

30. R. E. Turner *et al*., Phys. Fluids **27**, 511 (1984).

31. H. X. Vu, D. F. DuBois, J. F. Myatt, and D. A. Russell, presented at the 41st Annual Anomalous Absorption Conference, San Diego, CA, 19–24 June 2011.

32. J. F. Myatt, J. Zhang, A. V. Maximov, R. W. Short, D. F. DuBois, D. A. Russell, and H. X. Vu, Bull. Am. Phys. Soc. **56**, 328 (2011).

33. J. Zhang, J. F. Myatt, A. V. Maximov, R. W. Short, D. F. DuBois, D. A. Russell, and H. X. Vu, Bull. Am. Phys. Soc. **57**, 299 (2012).

34. J. Delettrez, R. Epstein, M. C. Richardson, P. A. Jaanimagi, and B. L. Henke, Phys. Rev. A **36**, 3926 (1987).